

# MALDI mass spectrometry based molecular phenotyping of CNS glial cells for prediction in mammalian brain tissue

Jörg Hanrieder · Grzegorz Wicher · Jonas Bergquist · Malin Andersson · Åsa Fex-Svenningsen

Received: 10 November 2010 / Revised: 9 April 2011 / Accepted: 18 April 2011 / Published online: 7 May 2011  
© Springer-Verlag 2011

**Abstract** The development of powerful analytical techniques for specific molecular characterization of neural cell types is of central relevance in neuroscience research for elucidating cellular functions in the central

Published in the special issue *MALDI Imaging* with Guest Editor Olivier Laprévotte.

**Electronic supplementary material** The online version of this article (doi:10.1007/s00216-011-5043-y) contains supplementary material, which is available to authorized users.

J. Hanrieder

Department of Pharmaceutical Bioscience, Drug Safety and Toxicology and Department of Physical and Analytical Chemistry, Analytical Chemistry, Uppsala University, PO Box 591, 75124 Uppsala, Sweden  
e-mail: jorg.hanrieder@kemi.uu.se

G. Wicher

Department of Genetics and Pathology, Cancer and Vascular Biology, Uppsala University, Rudbecklaboratoriet, 751 85 Uppsala, Sweden

J. Bergquist (✉)

Department of Physical and Analytical Chemistry, Analytical Chemistry, Uppsala University, PO Box 599, 75124 Uppsala, Sweden  
e-mail: jonas.bergquist@kemi.uu.se

M. Andersson (✉)

Department of Pharmaceutical Bioscience, Drug Safety and Toxicology, Uppsala University, PO Box 591, 75124 Uppsala, Sweden  
e-mail: malin.andersson@farmbio.uu.se

Å. Fex-Svenningsen (✉)

Institute of Medical Biology, Neurobiology Research, University of Southern Denmark, J.B. Winslows Vej 21, 1st floor, Dk-5000 Odense, Denmark  
e-mail: aasvenningsen@health.sdu.dk

nervous system (CNS). This study examines the use of differential protein expression profiling of mammalian neural cells using direct analysis by means of matrix-assisted laser desorption/ionization time-of-flight mass spectrometry (MALDI-TOF-MS). MALDI-MS analysis is rapid, sensitive, robust, and specific for large biomolecules in complex matrices. Here, we describe a newly developed and straightforward methodology for direct characterization of rodent CNS glial cells using MALDI-MS-based intact cell mass spectrometry (ICMS). This molecular phenotyping approach enables monitoring of cell growth stages, (stem) cell differentiation, as well as probing cellular responses towards different stimulations. Glial cells were separated into pure astroglial, microglial, and oligodendroglial cell cultures. The intact cell suspensions were then analyzed directly by MALDI-TOF-MS, resulting in characteristic mass spectra profiles that discriminated glial cell types using principal component analysis. Complementary proteomic experiments revealed the identity of these signature proteins that were predominantly expressed in the different glial cell types, including histone H4 for oligodendrocytes and S100-A10 for astrocytes. MALDI imaging MS was performed, and signature masses were employed as molecular tracers for prediction of oligodendroglial and astroglial localization in brain tissue. The different cell type specific protein distributions in tissue were validated using immunohistochemistry. ICMS of intact neuroglia is a simple and straightforward approach for characterization and discrimination of different cell types with molecular specificity.

**Keywords** Intact cell mass spectrometry (ICMS) · MALDI-TOF-MS · Imaging mass spectrometry (IMS) · Glial cells

## Introduction

In the human brain, nine out of ten cells are glial cells. Glial cells provide the brain with support trophic factors and are involved in basically all processes in brain transmission [1–5]. The various types of glial cells differ from each other in protein expression, function, and morphology, but much less is known about their function than that of neurons. Astrocytes contribute to synapse formation, intercellular communication, and regulation of neurotransmitter and ion homeostasis [4, 6, 7]. Oligodendrocytes produce myelin sheaths that increase signal propagation and may be important for the survival of neurons [8, 9]. As a large number of oligodendrocyte precursors are distributed uniformly throughout the gray and white matter of the mature central nervous system (CNS), they may also have other functions yet to be discovered. Microglia, the tissue-specific resident macrophages of the CNS, exists in all parts of the brain as well as spinal cord [10, 11]. Accumulating evidence suggests that alterations of neuron–glia interactions are associated with the development of most neurodegenerative diseases [12–17]. Oligodendrocytes and microglia are involved in multiple sclerosis, where oligodendrocytes are attacked by the immune system and microglia act as phagocytes [18, 19]. Astrocytes may play a role in neuroinflammation in Parkinson's disease [20] and are also involved in the formation of glial scars after injuries to the CNS, termed gliosis [21, 22]. In order to better understand the pathology of neurodegenerative diseases and injuries, one first has to delineate the responses of the different cell species as well as the nervous system as one organ.

The development of powerful techniques that facilitate rapid, sensitive, and specific cellular characterization is of great interest in current molecular neurobiology. Disease or trauma-induced protein changes of the CNS can be studied using mass spectrometry (MS). Proteins that are found to exhibit characteristic changes may serve as diagnostic markers as well as therapeutic targets for neuroprotection [23] and maintenance of the healthy CNS [9, 24, 25].

Direct analysis of intact cells by means of matrix-assisted laser desorption/ionization time-of-flight (MALDI-TOF) MS is an emerging technique for routine characterization of prokaryotic cultures. Intact cell mass spectrometry (ICMS) allows high throughput identification of bacterial species with high specificity based on their characteristic protein/peptide mass profiles [26]. The main feature of this approach is the simple sample handling, where only limited sample amounts are required ( $10^6$ – $10^7$  cells), easily obtainable from most routine cell preparation protocols. Commercial solutions for ICMS-based bacteria identification have been introduced and include the instrumental platform as well as software tools and a reference database [27]. Even though ICMS is a well-recognized approach for analysis of prokaryotic species, very

few studies on eukaryotic cell characterization have so far been reported [28–31].

The objective of this study was to establish an ICMS protocol for analysis of different types of glial cells. For this investigation, we chose to evaluate astrocytes, oligodendrocytes, and microglia from the rodent brain. By analyzing pure fractions of different cell species, we aimed to acquire template spectra for the different cell types.

The aim was therefore to establish and optimize a rapid and simple approach for direct analysis of intact rodent glial cells that allows differentiation of glia types based on characteristic protein and peptide mass fingerprint spectra. A further aim is the identification of cell specific protein markers that facilitate the prediction of the corresponding cellular phenotypes in brain tissue using MALDI imaging mass spectrometry (IMS; schematic overview in Electronic Supplementary Material Fig. S1).

## Materials and methods

### Chemicals

All chemicals were purchased from Merck (Darmstadt, Germany) unless otherwise stated. Leibovitz's L-15 medium, Dulbecco's modified Eagle's medium, and fetal calf serum glutamine were bought from Invitrogen (Stockholm, Sweden). Trifluoroacetic acid (TFA), penicillin-streptomycin, urea, dithiothreitol (DTT), 2',4',-dihydroxyacetophenone (DHAP), and iodoacetamide (IAA) were obtained from Sigma-Aldrich (Stockholm, Sweden). Water was purified with a Milli-Q (Millipore, Bedford, MA, USA) purification system. Sinapinic acid (SA), 2,5-di-hydroxy benzoic acid (DHB), peptide, and protein calibration standards were purchased from Bruker Daltonics (Bremen, Germany).

### Brain tissue and glial cells

The study was approved by the Regional Ethics Committee for Research on Animals in Uppsala (Sweden) and carried out in accordance with the policy of the Society for Neuroscience. To obtain brain tissue for immunochemical analysis, adult Sprague–Dawley rats from Tachonic (Lille Skensved, Denmark) were sacrificed by an overdose of CO<sub>2</sub>; the brains were rapidly dissected and frozen on dry ice. Coronal sections (14 μm) were cut on a cryostat (bregma from 2.04 to –2.52) [32] and stored at –20 °C prior to immunolabeling.

To obtain separate microglial, astroglial, and oligodendroglial cell suspensions, we used a modified version of the method previously described by McCarthy and de Vellis in 1980 [33]. In brief, the cultures were prepared from both cerebral hemispheres of newborn Sprague–Dawley rat pups (postnatal day 1 or 2) and placed in a 100-mm Petri dish with cold Leibovitz's

L-15 medium. Brain tissue was mechanically dissociated through a glass Pasteur pipette and passed through a 70- $\mu$ m nylon cell strainer (BD, Stockholm, Sweden) to remove all large fragments. Dissociated cells were washed twice in cold L-15 and centrifuged for 10 min at 1,000 rpm to remove debris.

After centrifugation, the cells were re-suspended in Dulbecco's modified Eagle's medium supplemented with 10% fetal calf serum, 0.3% L-glutamine, and 1% penicillin-streptomycin (all from Invitrogen, Stockholm, Sweden). Cells were then plated at a density of  $2 \times 10^5$  cells/cm<sup>2</sup> on poly-L-lysine-coated 75-cm<sup>2</sup> cell Falcon cell culture flasks (Fisher Scientific, Gothenburg, Sweden).

After 7–9 days, the culture flasks were placed in an oscillatory shaker (Innova 40, New Brunswick Scientific, Edison, NJ, USA) and shaken at 200 rpm with a 1.5-in. stroke diameter at 37 °C for 6 h. After this primary shaking procedure, the culture medium containing microglia was aspirated. Fresh media was added to the flasks, which were then returned to the shaker for 18 h. After 18 h, the oligodendrocyte precursors residing in the culture had detached and can thus be aspirated together with the medium. Remaining astrocytes were scraped from the bottom of the flask and diluted with fresh media. The suspensions of the different glial cells (microglia, oligodendrocytes, and astrocytes) reach a purity of 98% [34]. The cells were then mechanically dissociated using a Pasteur pipette and filtered through a 70- $\mu$ m nylon cell strainer (BD, Stockholm, Sweden). A total cell count to determine the number of cells in each fraction was performed using direct microscopic observation in a Bürker chamber (VWR, Darmstadt, Germany). The cells were rinsed three times with 150 mM ammonium acetate (AmAc), centrifuged at 1,000 rpm, and re-suspended in 150 mM AmAc to a final concentration of 25,000 cells/ $\mu$ L.

## Intact cell MALDI-TOF-MS

### *Sample preparation*

For intact protein analysis, a sandwich target preparation method using sinapinic acid (SA) was applied. Here, a polished steel target was prespotted with 1  $\mu$ L of SA matrix solution I (1 mg/mL; 100% acetonitrile (ACN)) to give a thin layer of matrix. A volume of 1  $\mu$ L cell suspension was mixed with 1.5  $\mu$ L SA solution II (10 mg/mL; 50%ACN/0.1%TFA), and 1  $\mu$ L of the cell/matrix mixture was spotted onto the thin layer matrix preparation. The matrix was allowed to co-crystallize with cells and then washed three times with 10  $\mu$ L ice-cold 0.1% TFA for salt removal.

### *MALDI-TOF-MS*

All samples were analyzed on an Ultraflex II MALDI-TOF/TOF mass spectrometer (Bruker Daltonics) equipped with a

smartbeam<sup>®</sup> laser. The mass range of 3 to 25 kDa was analyzed in linear positive mode and delayed extraction of 100 ns. A number of 1,000 shots were acquired automatically in 100-shot intervals in a random pattern throughout the sample spot.

### *Data processing*

All spectra were baseline subtracted (Convex Hull V3) and externally calibrated from calibration spots adjacent to the sample spots (FlexAnalysis v. 3.0, Bruker Daltonics). The spectra were exported in .dat and further processed using the PDS software (Medicwave AB, Halmstad, Sweden). Here, all spectra were normalized by their total ion current (TIC), before peak picking (S/N>3) and data binning (AUC). The resulting data were evaluated in Microsoft Excel (v. 2007) and Origin Pro (v.8.1, OriginLab, Northampton, MA, USA) for statistical evaluation by means of Student's *t* test and analysis of variance (ANOVA) followed by post hoc analysis using HSD Tukey. Principle component analysis (PCA) was performed using the Unscrambler X software (CAMO Inc., Oslo, Norway).

## Protein identification

### *SDS-PAGE and in-gel digestion*

Mixed glial cells ( $10^6$  cells) were lysed by sonication for 30 min in 50% ACN. The suspension was centrifuged at 10,000 $\times g$  for 10 min, and the supernatant was collected. For protein precipitation, six volumes of ice-cold acetone were added to the supernatant, and the sample was incubated at –20 °C overnight. The sample was centrifuged at 10,000 $\times g$  for 10 min, and the supernatant was removed. The precipitated protein fraction was reconstituted in 1 mL 1% acetic acid (HAc), and multiple 55- $\mu$ L aliquots were taken and mixed with 25  $\mu$ L XT sample buffer (Bio-Rad, Hercules, CA, USA), followed by 10  $\mu$ L 55 mM DTT. The samples were denatured at 95 °C for 5 min. For alkylation, a volume of 10  $\mu$ L 100 mM IAA was added followed by incubation for 10 min at room temperature in darkness. One dimensional gel electrophoresis was performed using the Criterion system (Bio-Rad) according to the manufacturer's instructions using commercial precast Criterion XT 4–12% Bis–Tris 18-comb gel and XT MES (Bio-Rad) running buffer. The gel was stained with Coomassie Blue R-250 (Bio-Rad).

Nine gel bands covering the region between 2.5 and 20 kDa were excised from the sodium dodecyl sulfate (SDS) gel according to the illustration in Electronic Supplementary Material Fig. S1. Gel cubes (2 $\times$ 2 $\times$ 2 mm) were digested with trypsin (100 ng/ $\mu$ L), in 50  $\mu$ L ammonium bicarbonate (50 mM) at 37 °C overnight. The digests were dried under vacuum, reconstituted in 10  $\mu$ L 1% HAc, and stored at

–20 °C until nanoscale liquid chromatography-electrospray tandem MS (nanoLC-ESI MS/MS) analysis.

#### NanoLC-ESI MS/MS

Reversed phase nanoLC-ESI MS/MS experiments were performed on an Ettan MDLC system (GE Healthcare, Uppsala, Sweden) hyphenated to an HCT ultra iontrap mass spectrometer (Bruker Daltonics). For reversed phase peptide separation, a dual column system was used consisting of a C18 trap column (Zorbax 300SB, 0.3×5 mm, 5 μm, Agilent Technologies, Santa Clara, CA, USA) for sample stacking and a C18 analytical column (Zorbax 300SB, 75 μm×150 mm, 3.5 μm, Agilent Technologies). A volume of 2.5 μL was automatically injected and separated using a water/acetonitrile/acetic acid gradient elution at a flow rate of 300 nL/min, starting at 1% HAc and a linear increase of ACN from 0% to 50% in 50 min. The nanoflow LC was interfaced to the mass spectrometer via a nano-electrospray ion-source (NanoSource I, Bruker Daltonics) using distal metal-coated emitter tips (20 μm, New Objective, Woburn, MA, USA) operating at a voltage of 1.5 kV at 200 °C. LC-MS/MS data was acquired using information-dependent product ion scan of three most intense peptide masses and processed in DataAnalysis (v. 3.4, Bruker Daltonics) by means of MS and MS/MS data extraction (Auto MSn), peak annotation, charge deconvolution, and export of detected compounds in .xml file format. The .xml datasets were submitted to comprehensive Mascot MS/MS search (v. 2.2, Matrix Science, Boston, MA, USA) using the BioTools software (v. 3.1 SR2; Bruker Daltonics) and the following specifications: species (*Rattus norvegicus*), fixed modifications (carbamidomethyl), variable modifications (oxidation M), mass tolerance-MS (1.5), mass tolerance-MS/MS (0.6 Da), enzyme (trypsin), missed cleavages (1), charge states (2<sup>+</sup>, 3<sup>+</sup>), and instrument (ESI-TRAP). The significance threshold was set to  $p < 0.05$ . MudPIT scoring was applied, requiring protein identification on at least one unique significantly identified peptide.

#### MALDI imaging

Striatal sections (12 μm) from fresh-frozen rat brain were cut on a cryostat and thaw-mounted on conductive glass slides for MALDI-IMS analysis (Bruker Daltonics). The sections were dried under vacuum and stored at –20 °C. Prior to matrix application, the sections were defrosted for 1 h and washed with 70% ethanol (EtOH) for 30 s, twice with 95% EtOH for 30 s, and dried in a vacuum desiccator. Sinapinic acid matrix (20 mg/mL SA, 50% ACN, 0.2% TFA) was applied with a resolution of 250 μm covering the whole brain section using a chemical inkjet printer (ChIP 1000, Shimadzu, Kyoto, Japan). A volume of 1,500 pL (15 drops) was applied per spot during each pass, and three passes of matrix application were performed. Data was acquired on an Ultraflex II MALDI-TOF/TOF instrument (Bruker Daltonics) running in linear positive mode using a delayed extraction of 100 ns. The mass range of 2–20 kDa was analyzed with a laser frequency of 100 Hz. A total sum of 200 shots per spot was acquired in steps of ten shots in a random pattern. Data sequence preparation and MS acquisition was performed using the FlexImaging software (v. 2.0, Bruker Daltonics).

#### Immunolabeling

The expression of different proteins was investigated using immunocytochemistry. After fixation, cells as well as cryosections (14 μm) were pre-incubated with blocking solution (1% bovine serum albumin (BSA), 0.3% Triton X-100, and 0.1% NaN<sub>3</sub> in PBS) for 1 h at RT. Incubation with primary antibodies (Table 1) diluted in blocking solution was performed overnight at 4 °C. The slides with cultures and brain sections were then washed 3×10 min in the washing solution (0.25% TritonX-100 in PBS), and secondary antibodies (anti-rabbit-Alexa488 or anti-mouse-RRX, Jackson Immuno Research Lab, Newmarket, UK) were diluted 1:200 in blocking solution and incubated for 4 h at RT. Samples were washed three times in PBS and mounted in DTG mounting media (2.5% DABCO, 50 mM Tris-HCl pH 8.0, 90% glycerol) with 0.375 ng/ml 4',6-diamidino-2-

**Table 1** Primary antibodies

Antibody name	Full name	Dilution	Species	Company of purchase
GFAP	Glial fibrillary acidic protein	1:500	Mouse	Sigma-Aldrich, Stockholm, Sweden
H3	Histone 3	1:200	Rabbit	Upstate/Millipore, Stockholm, Sweden
H4(K12)	Histone 4 (acetyl K12)	1:200	Rabbit	Cell Signaling Technology, Boston, MA, USA
H4(K8)	Histone 4 (acetyl K8)	1:200	Rabbit	Cell Signaling Technology, Boston, MA, USA
NG2	Chondroitin sulfate proteoglycan	1:500	Mouse	Millipore, Stockholm, Sweden
S100A10	S100 calcium binding protein A10	1:200	Chicken	Abcam, Cambridge, UK

phenylindole (DAPI), to visualize cell nuclei. Samples were analyzed using an Olympus fluorescent microscope and the Velocity software (Perkin Elmer, Stockholm, Sweden). The images were processed and arranged in Adobe Photoshop CS2.

## Results

### Sample preparation for intact cell MALDI-MS

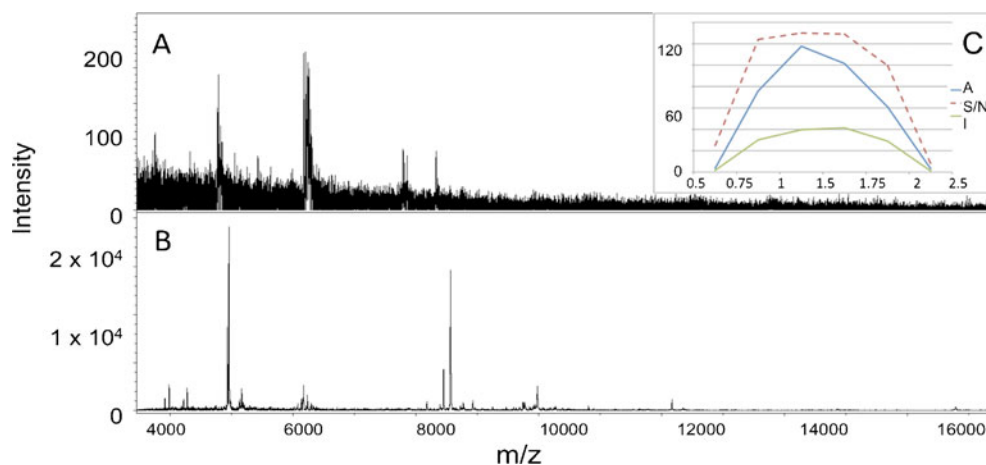
A mixed culture containing astrocytes, oligodendrocytes, and microglia was used for initial experiments to optimize sample handling and target preparation (Electronic Supplementary Material Fig. S1A). Mammalian cells are typically cultured in serum containing growth media (e.g., fetal calf serum) to optimize cell growth and survival. Extensive washing steps, often using PBS, are required prior MS analysis to avoid contamination from serum proteins. MALDI-MS is recognized to be a robust technique that is relatively tolerant towards salt impurities while maintaining its sensitivity. However, initial experiments of ICMS after PBS washing demonstrated that PBS impaired protein analysis (Fig. 1A). For this reason, PBS was replaced by 150 mM ammonium acetate (AmAc) as the washing agent. AmAc allows removal of media contamination while maintaining the cellular integrity similarly to PBS. When substituting the washing solution to AmAc, a dramatic improvement in spectra quality was observed (Fig. 1B). An optimal target preparation protocol was determined by comparing several commonly used techniques for sample and matrix application including thin layer preparation, dried droplet, and co-crystallization approaches. The best results were obtained for using the sandwich method, which includes initial application of matrix solved solely in highly volatile organic modifier such as acetone or methanol. This results in formation of a very thin and homogeneous matrix

layer that is referred to as thin layer or seed layer. Prior to the application of analyte to the target, the sample is mixed with matrix solution, and 1  $\mu\text{L}$  of the sample/matrix solution is spotted onto the seed layer for homogeneous co-crystallization. For determination of the optimal matrix/sample concentration ratio, a volume of 1  $\mu\text{L}$  cell suspension (25,000 cells/ $\mu\text{L}$ ) was mixed with different amounts of SA matrix solution prior spotting onto the MALDI target plate. The optimum peak intensity, peak area, and signal-to-noise ratio were 1.5  $\mu\text{L}$  SA solution per 1  $\mu\text{L}$  cell suspension (25,000 cells), corresponding to a total concentration ratio of 6  $\mu\text{g}$  SA/10,000 cells (Fig. 1C).

### Intact cell MS of neuroglia

The optimized sample preparation protocol was applied for all three different glial cell populations. The results demonstrate spectra that are characteristic for each cell species, as illustrated in Fig. 2A, B. The reproducibility was evaluated by means of peak intensity deviation analysis within each cell population. After MS normalization, an overall 25.9% relative standard deviation (RSD) was observed for all repetitive measurements for each cell type. A total of 237 protein peaks that had a signal-to-noise ratio of more than three was present in more than 10% of all spectra (a total of 60 spectra consisting of two biological repeats  $\times$  10 technical repeats  $\times$  3 cell types). Most protein peaks (232/237) displayed differential cell type abundance profiles on a 99% significance level (ANOVA,  $p < 0.01$ ). PCA revealed that the replicates from each cell types clustered together (Fig. 2C). The PCA data allowed identification of mass peaks that were predominantly increased for one cell type compared to the other two cell populations (Fig. 2C, D). The PCA loading plot (Fig. 2D) identified 76 peaks for astrocytes, 45 for oligodendrocytes, and 29 for microglia that were characteristically elevated in one cell type in contrast to both of the other two cell populations. Of these peaks, a number of 74

**Fig. 1** Ammonium acetate buffer improves MS quality. (A) Typical protocol involving trice washing with PBS for maintaining cell integrity. (B) Substitution of PBS by 150 mM ammonium acetate results in dramatic improvement of spectral quality. (C) Optimization of matrix: analyte display higher peak intensities (*I*), signal-to-noise ratio (*S/N*), and peak area (*A*) between 1 and 1.75  $\mu\text{L}$  MALDI matrix per microliter cell suspension



protein peaks displayed >2-fold change relative to the other two cell populations.

Even though a certain number of observed protein peaks could be assigned due to their accurate mass and with reference to previously published data (Table 2), these findings had to be validated using more extensive protein identification approaches. Therefore, a bottom-up proteomic approach based on 1D SDS-polyacrylamide gel electrophoresis (PAGE) and nanoLC-ESI-MS/MS was used for analyzing proteins from a glial cell lysate (Electronic Supplementary Material Fig. S1B). The MS/MS analysis resulted in unambiguous identification of 132 proteins (Electronic Supplementary Material Table S1). The LC-MS/MS results of each excised gel fraction representing a certain mass range were compared to the intact protein mass values obtained by MALDI-ICMS. Here, the results obtained by bottom-up proteomic analysis confirmed the presence of protein identities that were preliminary assigned due to their accurate intact masses (Table 2).

Interestingly, MALDI-MS profiling analysis revealed a four- to fivefold higher peak intensity/cell for histone protein masses, including histone H2A, H2B, H31, H33, and H4 in oligodendrocytes compared with astrocytes and microglia (Electronic Supplementary Material Fig. S2). Particularly, mass peaks of 11,308 and 11,350 Da were found to appear predominantly elevated in oligodendrocyte spectra and are suggested to match the histone H4 (2× methylated and singly acetylated, 11,308, H4(Ac); doubly acetylated, 11,350, H4(2Ac); Fig. 2B, arrow; Table 2). Peak intensities of several other proteins were increased in astrocytes compared relative to both oligodendrocytes and microglia (Electronic Supplementary Material Fig. S2). These included cytochrome C oxidase (COX), cytochrome C, ubiquitin, chaperonin 10, macrophage inhibitor factor, acetyl co-A binding protein, thioredoxin, calmodulin, S100 alpha 10, thymosin beta-10, and ribosomal protein S28 (Table 2 and Electronic Supplementary Material Fig. S2).

### Immunocytochemistry

Double immunochemistry was used to investigate if proteins that had been assigned to certain glial species using MALDI-MS also could be identified in the different glial cell types (Electronic Supplementary Material Fig. S1C). The mixed cultures used for immunocytochemistry were the same type of cultures as the ones previously used for MALDI-MS optimization. Since these cultures were generated from P1 rat pups, it was assumed that a majority of the oligodendroglial cells would be immature. For this reason, NG2, a marker for oligodendrocyte precursors, was used to identify oligodendroglial cells. For astrocytes, glial fibrillary acidic protein (GFAP) was used as cell marker. The MALDI-ICMS data showed a fivefold higher intensity of histone H4 in

**Fig. 2** Intact cell mass spectrometry (ICMS) on glial cells. **(A)** Characteristic fingerprint spectra for astrocytes (*I*), microglia (*II*), and oligodendrocytes (*III*). **(B)** The *insert* displays the peak at 11,308 and 11,350 Da, corresponding to histone H4 and its acetylated isoform in oligodendrocyte spectra (*arrow*). Intensity values on the *y*-axis are represented in arbitrary units, and *x*-axis corresponds to mass to charge range (*m/z*). **(C)** Principle component analysis on binned data from ten replicate analyses of each cell type reveals characteristic clustering of different glia cell types (scoring plot PC2/PC1). An average of about 25% CV demonstrates a high degree of precision of MALDI-ICMS and was evaluated between technical replicates. **(D)** The loading plot reveals peaks that can be used to discriminate and identify each glial cell population. *A*, astrocytes; *M*, microglia; *O*, oligodendrocytes

oligodendrocytes compared to astrocytes (Fig. 3A). This was not completely in accordance with the immunocytochemical results obtained from the cell cultures. Using immunocytochemistry for acetylated histone H4, it was found that H4(K8) as well as H4(K12) is also expressed in approximately 10–15% of the astrocyte population (Fig. 3B, D). Interestingly, only approximately 10% of the NG2-positive oligodendrocytes were positive for H4(K8) or H4(K12), but a higher degree of immunoreactivity in NG2-positive cells indicated a higher concentration of acetylated histone H4 (Fig. 3C, E). Here, higher levels of immunoreactivity were observed for the K12 acetylated H4. It is also possible that the MALDI-ICMS results reflect H4 acetylations of other sites beyond lysine 8 and 12, e.g., on lysine 6, 17, and 20, or a di-methyl H4(K20). While the MALDI results only indicate the presence of single or multiple post-translational modifications, immunocytochemistry experiments allow for distinct annotation of the respective modified amino acid residue if there is an antibody available. This further highlights the strength of this complementary approach, combining ICMS and immunocytochemistry.

The ICMS data also showed a fivefold higher peak intensity of H3 (Fig. 4A) in oligodendrocytes. Double immunolabeling using an H3 antibody with GFAP (Fig. 4B) and NG2 (Fig. 4C) failed to demonstrate higher histone H3 levels in any glia cell type. However, a large number of H3-positive cells in these cultures were neither labeled for GFAP nor NG2. This might be a direct consequence of the limited specificity of the H31 antibody that has been used for these experiments, which is directed towards multiple isoforms of H3 including H31, H33, and H3c2. This lack in specificity leads to a drowning effect and significant dilution of the H31 immunoreactivity. Another possible explanation could be that these cells are most likely stem cells and may have contributed to the increased peaks in the ICMS data for oligodendrocytes. These cells are often present together with the oligodendrocytes in the cultures and may be shaken off together with the oligodendrocyte fraction (data not shown). The here presented results on immunohistochemical histone characterization in mixed cell cultures demonstrate the need for appropriate antibody

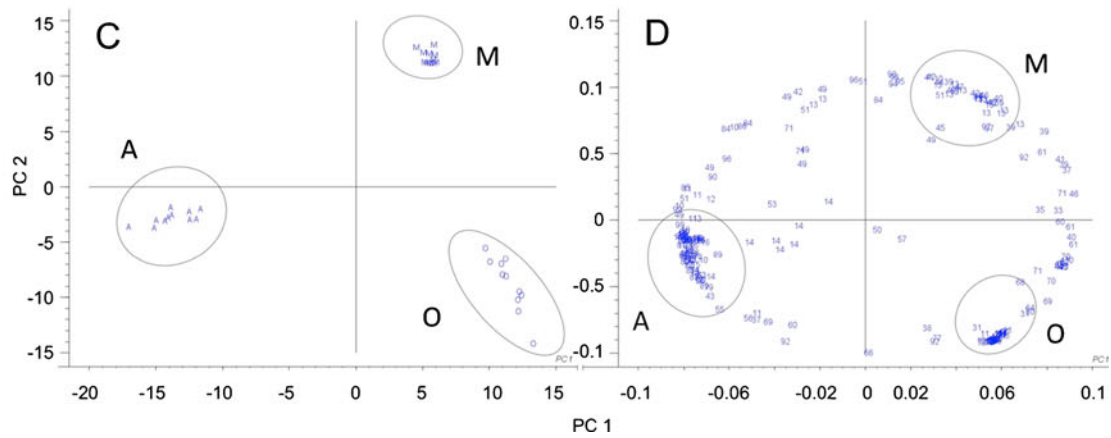
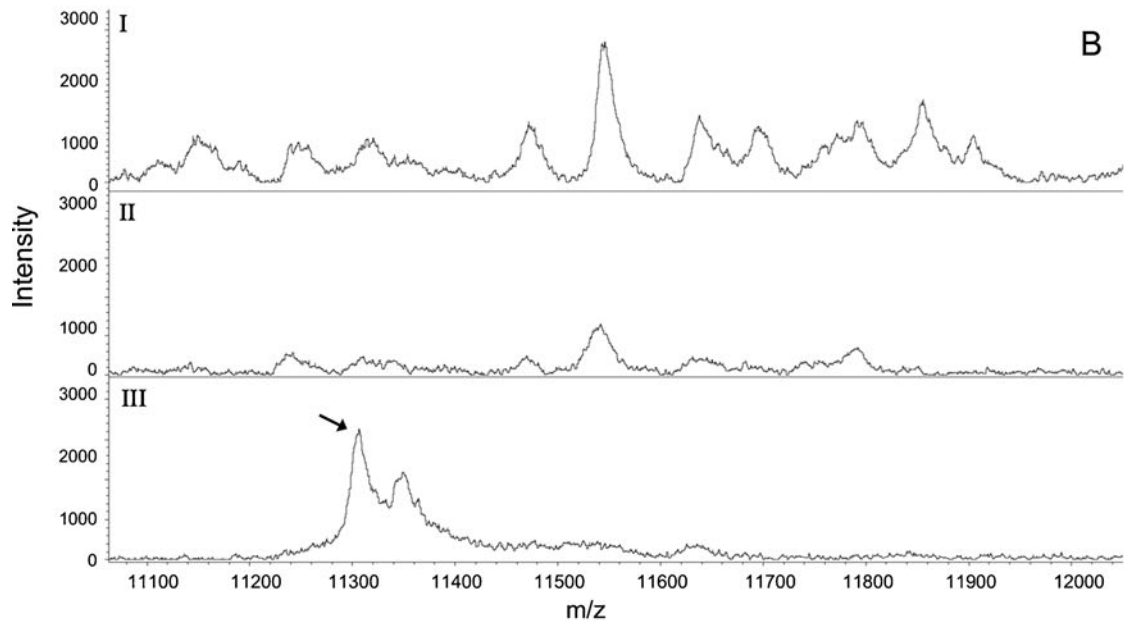
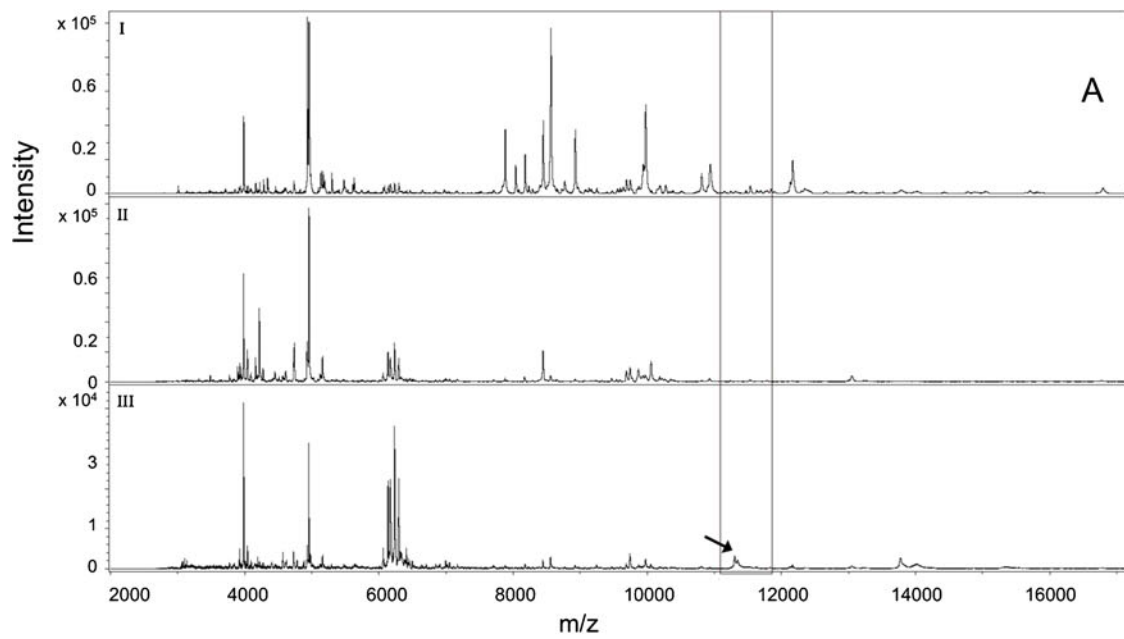


**Table 2** Mass matched proteins identified by bottom-up proteomics

Name	Entry <sup>a</sup>	Mass [M+H] <sup>+</sup> <sup>b</sup>		Modifications <sup>c</sup>
		Calculated	Observed	
Acyl-CoA binding protein	ACBP_RAT	9,940	9,940	N-term. Ac
Calmodulin	CALM_RAT	16,783	16,787	N-term. Ac, N6,N6 dimethyl Lys,
Chaperonin 10	CH10_RAT	10,812	10,811	N-term. Ac
Cytochrome C oxidase	COX_RAT	9,979	9,979	N-term Ac+2 disulfide bonds
Cytochrome C oxidase 7A	CX7A2_RAT	6,648	6,648	-propeptide
Cytochrome B	CYTB_RAT	11,240	11,240	N-term-Ac
Cytochrome C	CYTC_RAT	12,132	12,132	Heme group, 1 Ac
Cytochrome C	CYTC_RAT	12,168	12,168	Heme group, 1xAc, 2xOx
FK506 binding protein 1A	FK506_RAT	11,791	11,793	-N-term. Met
Histone 4	H4_RAT	11,308	11,308	2xMeth, 1xAc
Histone 4	H4_RAT	11,350	11,350	2xMeth, 2xAc
Histone H2A type 1-C	H2A1C_RAT	14,016	14,014	N-term. Ac
Histone H2A type 1-C	H2A1C_RAT	14,048	14,047	N-term. Ac+2Ox
Histone H2B type 1	H2B1_RAT	13,778	13,776	See reference [34]
Histone H2B type 1	H2B1_RAT	13,818	13,816	1xAc
Histone H3.1	H31_RAT	15,336	15,338	N-term. Ac, Na-adduct
Histone H3.1	H31_RAT	15,354	15,357	N-term.-Ac 1xOx
Histone H3.1	H33_RAT	15,378	15,376	N-term. Ac, 1xAc
Macrophage inhibitory factor	MIF_RAT	12,347	12,347	-N-term. Met
Protein S100-A10	S10AA_RAT	10,940	10,939	-N-term. Met
Ribosomal protein S28	RS28_RAT	7,885	7,885	1xAc
Thioredoxin	THIO_RAT	11,542	11,542	N-term. Ac
Thymosin beta 10	TYB10_RAT	4,936	4,936	N-term. Ac
Thymosin beta 4	TYB4_RAT	4,963	4,963	N-term. Ac
Ubiquitin	UBC_RAT	8,565	8,565	-

<sup>a</sup> Database entry from the uniprot knowledgebase ([www.uniprot.org](http://www.uniprot.org))

<sup>b</sup> Observed and theoretical mass to charge values of the matched protein identities

<sup>c</sup> Known modifications of the proteins as listed in the uniprot database that were found to match the observed protein sequences. Observed masses could be re-calculated with these modifications based on the theoretical mass. N-terminal acetylation implies always removal of N-term. methionine

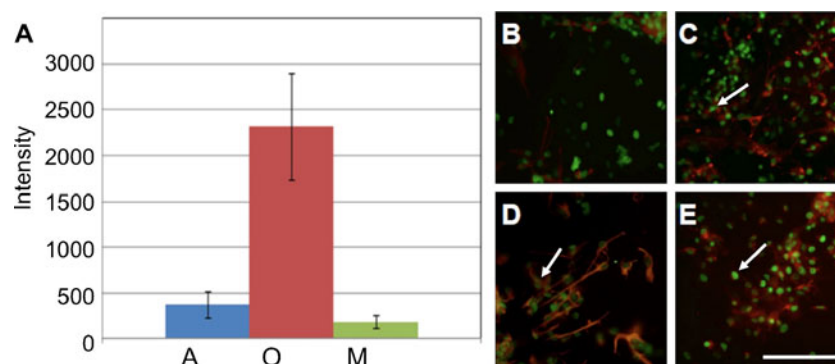


**Fig. 3** IHC analysis of histone H4 in mixed glia cell cultures. (A) MALDI-MS analysis shows fivefold higher peak intensity of histone H4 in oligodendrocytes compared to astrocytes (error bars indicate standard deviation, n=10). (B–E) Double antigen immunocytochemistry for astrocytes (GFAP in red; B, D), oligodendrocytes (NG2 in red, C, E), and histone H4 acetylation of lysine 8 (K8; B, C) and 12

(K12; D, E). About 10–20% of both oligodendrocytes and astrocytes were positive for acetylated histone H4; however, higher immunoreactivity was detected in oligodendrocytes (arrow, C, E) compared to H4-positive astrocytes (arrow, D). A, astrocytes; M, microglia; O, oligodendrocytes; scale bar, 100 μm



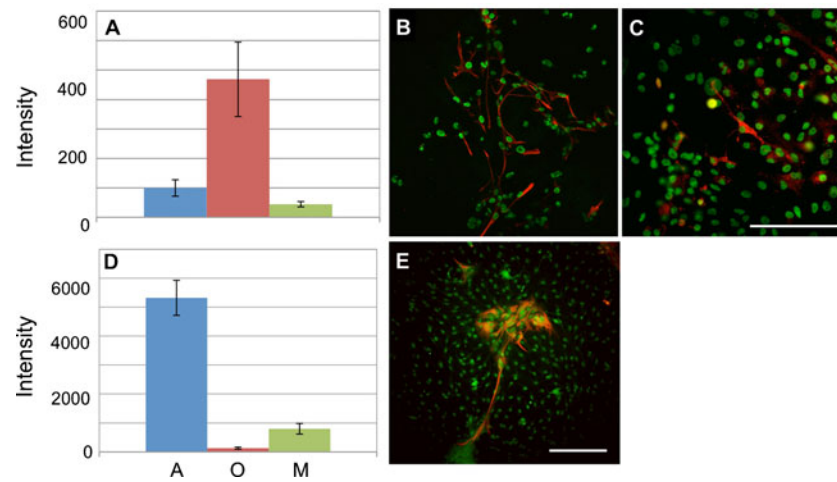


**Fig. 4** Histone H3 and S100-A10 in mixed cultures. **(A)** Quantification of MALDI data shows fivefold higher peak intensity/cell of histone H3 protein in oligodendrocytes compared to the other two glia cell types (error bars indicate standard deviation,  $n=10$ ). **(B, C)** Double labeling of histone H3 (green) with either GFAP (red; **B**) or NG2 (red; **C**) shows co-labeling for the majority of both glia types.

**(D)** A >10-fold higher MALDI peak intensity for S100-A10 was detected in astrocytes compared with oligodendrocytes and microglia. **(E)** Indeed, strong co-labeling for S100-A10-IR (green) and GFAP (red) was detected in astrocytes. A, astrocytes; M, microglia; O, oligodendrocytes; scale bar, 100  $\mu\text{m}$

specificity and a multitude of functional and specific cell markers. The data from the intact cell MALDI-MS displayed a fivefold higher peak intensity/cell of S100-A10 protein in astrocytes (Fig. 4D). Using an antibody for S100-A10, it was found that this finding was in accordance with our MALDI-MS data. Double-labeling using S100-A10 with GFAP demonstrates that a majority of GFAP-positive astrocytes are S100-A10-positive (Fig. 4E).

#### MALDI imaging mass spectrometry

Striatal sections of adult rat brain were analyzed by means of MALDI-IMS and immunohistochemistry (IHC), respectively. Several peaks localize to specific brain tissue regions, such as the corpus callosum and ventricles,  $m/z$  11,308 (histone H4); grey matter,  $m/z$  7,725 (guanine nucleotide-binding protein G (I)/G(S)/G(O) subunit gamma-2; GNG2) [35]; or striatum,  $m/z$  7,383 (GNG7) [36] (Fig. 5). Moreover, the distribution of the targeted identifier masses deduced from the ICMS experiments could be displayed. High peak intensities of both histones H4 and H31 and their multiple-acetylated isoforms were consistently observed in the corpus callosum and in close proximity to lateral ventricles, as well as medial part of caudate putamen (Fig. 6A, B). The antibodies for H4 (2 $\times$  acetylated isoform, H4(2Ac)) and H3 (singly acetylated, H31(Ac)) displayed nuclear labeling throughout adult brain tissue, but in particular, intense immunolabeling for the two forms of H4(2Ac) and H31(Ac) histone was found around the ventricles, including the sub-ventricular zone and the medial caudate putamen of adult rat brain confirming MALDI imaging analysis (Fig. 6C, D). To further characterize H4(2Ac)- and H31(Ac)-positive cells in tissue, we

used double-immunolabeling with known glial markers (GFAP and NG2). Oligodendrocyte analysis of brain tissue showed that most of H4(2Ac) and H31(Ac)-IR cells in the white matter (corpus callosum) were indeed positive for NG2 in adult brain (Fig. 6E, F).

#### Discussion

In the present study, a MALDI-MS-based approach for fast and robust identification of intact eukaryotic cells is presented (Electronic Supplementary Material Fig. S1). While MALDI-MS-based analysis of microorganisms has been well established for bacteria strain identification, where it is currently validated for clinical application [26], there are few reports on direct analysis of intact mammalian cells using MALDI-MS [29, 31]. A main obstacle has been that cell culturing medium contains large amounts of biological and chemical additives that interfere with MS, in particular, proteins originating from serum may bias the analysis. Therefore, extensive washing while maintaining cellular integrity is necessary. Typically, PBS is used for removing excessive medium compounds prior MALDI analysis, since it is providing physiological pH and ionic strength that maintains cellular integrity. However, PBS is not optimal for MALDI-MS, due to its content of phosphate ions and sodium chloride. Here, we demonstrate that a significant increase in spectral quality was obtained by replacing PBS with 150 mM ammonium acetate buffer at physiological pH and ionic strength. The volatility of the acetate buffer results in little or no interferences with sample ionization efficiency compared with PBS [37].

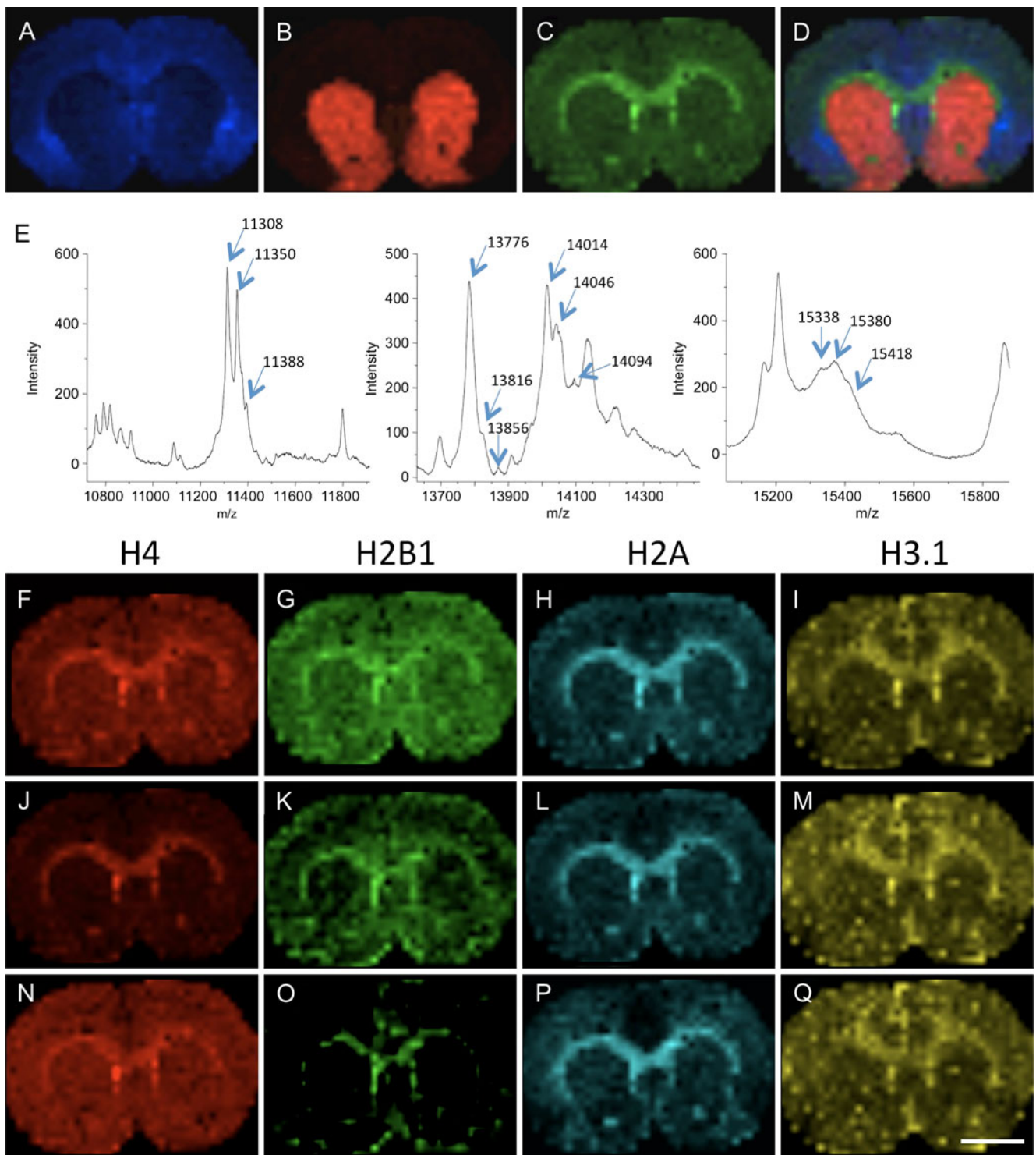
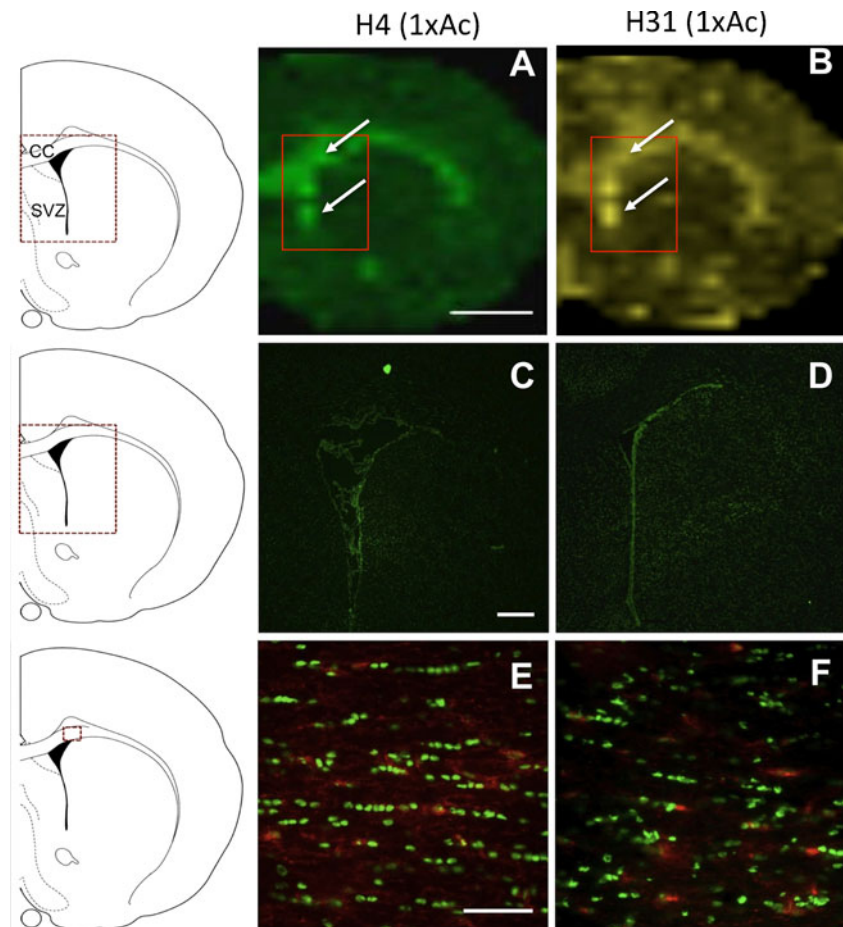


**Fig. 5** MALDI imaging mass spectrometry of a rat brain section. (A) Guanine nucleotide-binding protein G(I)/G(S)/G(O) subunit gamma-2 (GNG2) is localized to the septum and cortical areas, whereas GNG7 is mainly distributed in the striatum (B). (C) Histone H4 distribution pattern in brain tissue. (D) The composite distribution map demonstrates high histone peak intensity in white matter fiber bundles and around the lateral ventricles. (E) Average MS trace of spectra from lateral ventricles and corpus callosum shows several peaks in close

association to the histones detected by ICMS (arrows), including histone H4 (F;  $m/z$  11,308), H2B1 (G;  $m/z$  13,776), H2A (H;  $m/z$  14,014), and H3.1 (I;  $m/z$  15,338). Ion distribution maps reveal close to identical anatomical localization of the peaks corresponding to +42 Da, suggesting 1 acetylation (J–M) and +80 Da, suggesting 1 phosphorylation (N–Q). MALDI matrix was printed at a spatial resolution of 175  $\mu\text{m}$  (scale bar=1 mm), and the maximum peak intensity in each image was set to 100%

**Fig. 6** MALDI imaging mass spectrometry and immunohistochemical localization of histones in rat brain. (A, B) MALDI imaging revealed acetylated histone H4 (H4-1Ac,  $m/z=11,308$ ; A) and H3 (H31-1Ac,  $m/z=15,357$ ; B) in the corpus callosum (CC) as well as in close proximity to lateral ventricles and medial part of caudate putamen (scale bar=1 mm). (C, D) In concordance with the MALDI-IMS results, intense immunolabeling for both H4 and H3 was detected in the sub-ventricular zone (SVZ) around the lateral ventricle (scale bar=500  $\mu\text{m}$ ). (E, F) NG2-immunopositive oligodendrocytes (displayed in red) co-express both H4 and H3 (green) in the corpus callosum (scale bar=50  $\mu\text{m}$ )



The performance of the demonstrated ICMS approach is primarily characterized by its robustness and its feasibility for fast, sensitive, and specific cell speciation analysis. The technique proved to be very reliable with respect to the observed reproducibility when applying spectra TIC normalization. In fact, the average TIC for ten replicates per group did not differ significantly between astrocyte and oligodendrocyte cell types. No overnormalization effects could be detected, as several of the assigned peaks were compared before and after TIC normalization, and the fold-change difference did not change, whereas the variability was reduced by 25%. This approach enables characterization of cell populations due to their exhibited mass signature spectra using multivariate statistics (Fig. 4C). Here, the protein mass peaks could be determined that exhibited the biggest differences in intensity and allowed the cell types to be significantly distinguished from each other (Fig. 4D).

Among these mass peaks, several protein identities could be initially assigned based on mass matching, using the mass accuracy of the TOF analyzer and their theoretical mass from database listed known sequence data, including known protein specific post-translational modifications (Table 2). However, protein identification is complicated by the fact that many post-translational truncations and

modifications are not yet known, making database searches impossible, and thus requiring de novo sequencing. Many groups have demonstrated that true top-down proteomic MS/MS analysis of highly abundant known peptides and smaller proteins is possible directly off tissue [34, 38–45]. However, top-down MS/MS analysis on higher molecular weight proteins is difficult because of the complexity of fragmentation pattern to be interpreted. Common proteomic strategies are typically based on enzymatic digestion and LC-MS/MS analysis of tryptic peptides, preferably after reduction of sample complexity by gel electrophoresis or liquid chromatography. For verifying our mass matching results, we performed bottom-up proteomic analysis using PAGE for sample complexity reduction. Since most proteins were present in all glial cell types, albeit at various concentrations, mixed glial cell lysates were used for protein identification. In order to cover the corresponding mass range examined by MALDI-MS, nine consecutive equidistant gel pieces below 20 kDa were excised, trypsinated, and further analyzed by means of nanoLC-ESI MS/MS (Electronic Supplementary Material Fig. S1B). These findings included, e.g., histone proteins (H2A, H2B, H31, H33, and H4), thymosins (beta 4 and 10), ubiquitin, and cytochrome C, which have all been reported previously

where they have been detected by MALDI-TOF-MS in rat brain tissue (Table 2) [46]. MALDI-IMS can be used for further verifying the protein identification with the intact mass observed, for example, all histones reported here displayed the same anatomical localization pattern in brain tissue (Fig. 5).

Several of these protein peaks exhibited significantly higher peak intensity in one specific glial cell population and may indicate actual differences in protein abundances for the different glial cell types (Electronic Supplementary Material Fig. S2). Histone H4 and histone H31 were found to be characteristically intense in ICMS spectra of oligodendrocytes and may therefore serve as specific cell marker (Figs. 2B, 3A, and 4A). Double immunolabeling using histone antibodies revealed no difference in the number of labeled astrocytes and oligodendrocytes; however, stronger histone H4 immunoreactivity was detected in oligodendrocytes than in astrocytes, which is in accordance with the findings of the ICMS experiments. However, one has to keep in mind that MALDI-MS is not an absolute quantitative technique due to ion-suppression effects originating from both different concentrations and ionization preferences of the analyte molecules depending on their chemical properties [47]. On the upside, ICMS data can serve as an initial hint for relative protein abundance that can be further verified using orthogonal techniques. Despite the mentioned limitations, MALDI-MS-based cell profiling features many advantages, like its robustness, speed, simplicity, sensitivity, and particularly, the feasibility of detecting multiple protein species in parallel. In contrast to the histone results S100-A10 was found predominantly elevated in astrocyte ICMS-data, and high immunoreactivity was observed in GFAP-positive astrocytes. These observations support the ICMS results and its potential for rough estimation of protein abundance in different cell populations but also highlight the need for orthogonal validation of MS-derived results on protein abundance changes in biological samples. Furthermore, the results obtained from the ICMS approach can reveal potential identifier masses for other MS-based investigations, such as MALDI-IMS for predicting cellular phenotypes in situ. To test this hypothesis, we performed MALDI imaging experiments on striatal sections of adult rat brain tissue. Mass peaks that were assigned as histones, predominantly abundant in the ICMS spectra of oligodendrocytes, were characteristically localized in the white matter (corpus callosum, Figs. 5 and 6A, B). Indeed, high H4 and H31 immunoreactivity was observed for NG2 immunopositive oligodendrocytes in the corpus callosum confirming the ICMS results (Fig. 6C–F). This is of particular interest since it is well known that oligodendrocytes are enriched in the corpus callosum, where they ensheath axons in myelin to ensure fast axonal transmission of electric signals. No distinct spatial distribution pattern was observed for S100-A10 (data not shown),

which is not surprising since astrocytes are evenly distributed in the brain and do not exert characteristic localization patterns except in for example brain injury.

Taken together, the improved methodology for cellular profiling proved to be a promising approach for the discrimination of different glial cell types due to their characteristic protein mass peak fingerprint. Furthermore, distinct signature proteins that constitute the most cell type characteristic feature, upon which the different cell types can be distinguished, could be identified. When performing MALDI-IMS, these signature masses could be employed as molecular cell markers in order to predict the respective cell types in brain tissue.

Providing the possibility for instantaneous localization and identification of complex protein composition, the presented MALDI-MS-based approach offers the unique possibility to analyze intracellular processes in health and disease.

## Conclusion

In conclusion, this elegant, quick, and sensitive method proved to be a suitable approach for neural cell profile characterization as demonstrated for neuroglia subtypes. Moreover, observation and identification of unique proteins, as well as changes in protein expression in vitro and in situ, may make this technique attractive as a future diagnostic tool in neuroscience research.

**Acknowledgements** The Swedish Research Council Grants 342-2004-3944 (JB), 621-2008-3562 (JB), 522-2006-6416 (MA), 521-2007-5407 (MA), and 2006-4268 (ÅFS); The Royal Swedish Academy of Sciences (MA, JH); Gyllenstiernska Krappertstiftelsen (ÅFS); Åhlenstiftelsen, Hjärnfonden (GW, postdoctoral); and the Swedish Chemical Society (JH) are gratefully acknowledged for financial support.

## References

1. Butt AM, Hamilton N, Hubbard P, Pugh M, Ibrahim M (2005) *J Anat* 207(6):695–706
2. Freeman MR (2006) *Curr Opin Neurobiol* 16(1):119–125
3. Perea G, Araque A (2005) *J Neurosci* 25(9):2192–2203
4. Ullian EM, Sapperstein SK, Christopherson KS, Barres BA (2001) *Science* 291(5504):657–661
5. Tan L, Sun S, Duan S, Wang X (2005) *J Huazhong Univ Sci Technolog Med Sci* 25(5):484–487
6. Christopherson KS, Ullian EM, Stokes CC, Mallowney CE, Hell JW, Agah A, Lawler J, Mosher DF, Bornstein P, Barres BA (2005) *Cell* 120(3):421–433
7. Seifert G, Weber M, Schramm J, Steinhauser C (2003) *Mol Cell Neurosci* 22(2):248–258
8. Bauer NG, Richter-Landsberg C, Ffrench-Constant C (2009) *Glia* 57(16):1691–1705
9. Barres BA (2008) *Neuron* 60(3):430–440
10. Mittelbronn M, Dietz K, Schluesener HJ, Meyermann R (2001) *Acta Neuropathol* 101(3):249–255
11. Graeber MB, Streit WJ (2010) *Acta Neuropathol* 119(1):89–105

12. Bradl M, Lassmann H (2009) *Semin Immunopathol* 31(4):455–465
13. Miller DW, Cookson MR, Dickson DW (2004) *Neuron Glia Biol* 1(1):13–21
14. Heneka MT (2009) *Exp Neurol* 217(2):237–239
15. Clement AM, Nguyen MD, Roberts EA, Garcia ML, Boillee S, Rule M, McMahon AP, Doucette W, Siwek D, Ferrante RJ, Brown RH Jr, Julien JP, Goldstein LS, Cleveland DW (2003) *Science* 302(5642):113–117
16. Boillee S, Vande Velde C, Cleveland DW (2006) *Neuron* 52(1):39–59
17. Bradl M, Lassmann H (2010) *Acta Neuropathol* 119(1):37–53
18. Jack C, Ruffini F, Bar-Or A, Antel JP (2005) *J Neurosci Res* 81(3):363–373
19. Piaton G, Williams A, Seilhean D, Lubetzki C (2009) *Prog Brain Res* 175:453–464
20. Chung YC, Ko HW, Bok E, Park ES, Huh SH, Nam JH, Jin BK (2010) *BMB Rep* 43(4):225–232
21. Eng LF, Ghimikar RS (1994) *Brain Pathol* 4(3):229–237
22. Sofroniew MV (2009) *Trends Neurosci* 32(12):638–647
23. Iizuka A, Takayama K, Torashima T, Yamasaki M, Koyama C, Mitsumura K, Watanabe M, Hirai H (2009) *Neurobiol Dis* 35(3):457–465
24. Jessen KR (2006) *Novartis Found Symp* 276:5–14, discussion 54–17, 275–281
25. Milligan ED, Watkins LR (2009) *Nat Rev Neurosci* 10(1):23–36
26. Fenselau C, Demirev PA (2001) *Mass Spectrom Rev* 20(4):157–171
27. Marvin LF, Roberts MA, Fay LB (2003) *Clin Chim Acta* 337(1–2):11–21
28. Bergquist J (1999) *Chromatographia* 49:S41–S48
29. Buchanan CM, Malik AS, Cooper GJ (2007) *Rapid Commun Mass Spectrom* 21(21):3452–3458
30. Kulkarni MJ, Vinod VP, Umasankar PK, Patole MS, Rao M (2006) *Rapid Commun Mass Spectrom* 20(18):2769–2772
31. Zhang X, Scalf M, Berggren TW, Westphall MS, Smith LM (2006) *J Am Soc Mass Spectrom* 17(4):490–499
32. Paxinos G, Watson C (2007) *The rat brain in stereotaxic coordinates*, 6th edn. Elsevier Academic, San Diego
33. McCarthy KD, de Vellis J (1980) *J Cell Biol* 85(3):890–902
34. Jespersen S, Chaurand P, van Strien FJ, Spengler B, van der Greef J (1999) *Anal Chem* 71(3):660–666
35. Mathur BN, Caprioli RM, Deutch AY (2009) *Cereb Cortex* 19(10):2372–2379
36. Skold K, Svensson M, Nilsson A, Zhang X, Nydahl K, Caprioli RM, Svenningsson P, Andren PE (2006) *J Proteome Res* 5(2):262–269
37. Keller BO, Suj J, Young AB, Whittal RM (2008) *Anal Chim Acta* 627(1):71–81
38. Jimenez CR, Li KW, Dreisewerd K, Spijker S, Kingston R, Bateman RH, Burlingame AL, Smit AB, van Minnen J, Geraerts WP (1998) *Biochemistry* 37(7):2070–2076
39. Kruse R, Sweedler JV (2003) *J Am Soc Mass Spectrom* 14(7):752–759
40. Kutz KK, Schmidt JJ, Li L (2004) *Anal Chem* 76(19):5630–5640
41. Li L, Garden RW, Romanova EV, Sweedler JV (1999) *Anal Chem* 71(24):5451–5458
42. Rubakhin SS, Greenough WT, Sweedler JV (2003) *Anal Chem* 75(20):5374–5380
43. Shimma S, Sugiura Y, Hayasaka T, Zaima N, Matsumoto M, Setou M (2008) *Anal Chem* 80(3):878–885
44. Andersson M, Groseclose MR, Deutch AY, Caprioli RM (2008) *Nat Meth* 5(1):101–108
45. Verhaert PD, Pinkse MW, Strupat K, Conaway MC (2010) *Meth Mol Biol* 656:433–449
46. Pierson J, Svenningsson P, Caprioli RM, Andren PE (2005) *J Proteome Res* 4(2):223–226
47. Stults JT (1995) *Curr Opin Struct Biol* 5(5):691–698